ELSEVIER

Journal of Structural Geology 29 (2007) 73–85

JOURNAL OF STRUCTURAL GEOLOGY

www.elsevier.com/locate/jsg

2-D and 3-D modeling of detachment folds with hinterland inflation: A natural example from the Monterrey Salient, northeastern Mexico

M. Scott Wilkerson [a,*], Sara M. Smaltz [a], Dannena R. Bowman [a], Mark P. Fischer [b], I. Camilo Higuera-Diaz [b]

[a] *Department of Geosciences, DePauw University, Greencastle, IN 46135, USA*
[b] *Department of Geology and Environmental Geosciences, Northern Illinois University, DeKalb, IL 60115, USA*

Received 1 February 2006; received in revised form 14 July 2006; accepted 14 July 2006
Available online 27 September 2006

Abstract

Geologists now recognize the presence and abundance of detachment folds in various contractional settings. Several two-dimensional geometric and kinematic models exist to describe the development of such structures. These models typically are area-balanced, are interpreted to develop by hinge migration, limb rotation, or a combination of the two processes, and possess a constant regional level outside the fold itself. We present two new two-dimensional geometric and kinematic models for detachment folds that incorporate hinge migration and limb rotation as their deformation mechanisms. These area-balanced models differ from previous models, however, in that they allow 'hinterland inflation' to occur, thereby creating a higher local regional level in the hinterland relative to the foreland. This local regional difference across the detachment fold may reflect hinterland uplift due to thickening of the incompetent unit, foreland deflation of the incompetent unit as material migrates into the fold core during fold growth, and/or migration of material out of the fold core as the fold tightens.

We illustrate the utility of these models by constructing pseudo-three-dimensional representations of the western termination of the Nuncios Fold Complex in the Monterrey Salient, northeastern Mexico. Our results suggest that the limb rotation model more accurately portrays the overall three-dimensional fold geometry for the Nuncios Fold Complex, matches the observed hinterland inflation, and predicts more reasonable detachment depths for the structure along its length. These results agree with interpreted kinematics based on field observations and illustrate how this modeling approach may help constrain interpretations of detachment folds with hinterland inflation in areas lacking sufficient data.

Keywords: Fault-related folds; Detachment folds; Monterrey Salient, Mexico; Kinematic model

1. Introduction

Maps and cross sections of most contractional settings commonly depict fault-related folds (e.g., fault-bend folds, fault-propagation folds, detachment folds) as fundamental structural elements that comprise these complex regions (e.g., Dahlstrom, 1970; Suppe, 1983; Jamison, 1987; Mitra, 1990, 1992; Suppe and Medwedeff, 1990; Wilkerson et al., 1991; Wilkerson and Wellman, 1993; Apotria and Wilkerson, 2002). Within the last two decades, geologists have come to recognize that detachment folds are more abundant and play a more significant role in these settings than previously thought (e.g., Jamison, 1987; Mitchell and Woodward, 1988; Dahlstrom, 1990; Epard and Groshong, 1993; Groshong and Epard, 1994; Hardy and Poblet, 1994; Epard and Groshong, 1995; Homza and Wallace, 1995; Poblet and Hardy, 1995; Poblet and McClay, 1996; Homza and Wallace, 1997; Atkinson and Wallace, 2003; Wilkerson et al., 2004). Detachment folds commonly develop to accommodate shortening and displacement of rocks with contrasting mechanical properties above (or below) a sub-horizontal slip surface (i.e., a detachment; Wilkerson et al., 2004). Typically, detachment folds

* Corresponding author. Tel.: +1 765 658 4666; fax: +1 765 658 4732.
E-mail addresses: mswilke@depauw.edu (M.S. Wilkerson), mfischer@niu.edu (M.P. Fischer).

0191-8141/$ - see front matter © 2006 Elsevier Ltd. All rights reserved.
doi:10.1016/j.jsg.2006.07.010

exhibit a box-fold geometry whose internal core contains an incompetent mechanical unit that may or may not deform disharmonically from the overlying competent mechanical layers (e.g., Fig. 1). In contrast to other types of fault-related folds, detachment folds lack a first-order fault ramp that steps up from the basal detachment surface.

Numerous two-dimensional geometric and kinematic models have been proposed to describe the development of detachment folds (e.g., Dahlstrom, 1990; Homza and Wallace, 1995; Poblet and McClay, 1996; Homza and Wallace, 1997; Atkinson and Wallace, 2003; Mitra, 2003). Most models create area-balanced cross sections of detachment folds (cf. Chamberlin, 1910) by prescribing geometric relationships between shortening, detachment depth, limb dips, and limb lengths due to the kinematic processes of hinge migration, limb rotation, or some combination of the two while maintaining a constant local regional stratigraphic level outside of the fold itself. Several authors (e.g., Homza and Wallace, 1997; Bulnes and Poblet, 1998; Wallace and Homza, 1998; Thomas, 2001; Mitra, 2003), however, have documented or hypothesized that the thickness of the incompetent layer may experience significant thickness changes during detachment fold development. Such changes may produce a corresponding deflation and/or inflation of the local regional stratigraphic level outside the bounds of the detachment fold anticline. In some cases, these changes are approximately equal on either side of the detachment fold anticline, whereas in others, the local regional levels exhibit differences in elevation between the hinterland and foreland (e.g., Homza and Wallace, 1997; Bulnes and Poblet, 1998; Wallace and Homza, 1998; Thomas, 2001; Mitra, 2003). Such differences in local regional levels across a fold may not exclusively reflect thickness changes in the detachment layer above a sub-horizontal detachment, but rather may also indicate fundamental differences in the underlying geological architecture (e.g., faulting, non-horizontal detachment, non-horizontal sub-detachment units, etc.).

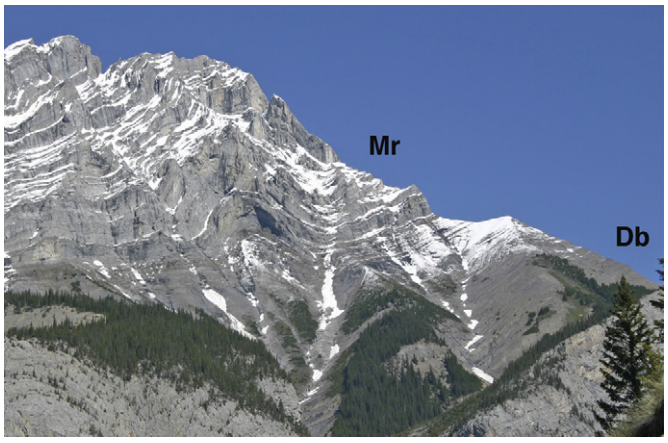

Fig. 1. Photo of detachment fold on the southeastern face of Cascade Mountain near Banff, Alberta, Canada. Mississippian Rundle Group (Mr) carbonate rocks define a small fold above a detachment within the shaly beds of the Devonian Banff Formation (Db). Structure lies within the hanging wall of the Rundle thrust sheet.

In this manuscript, we describe two new two-dimensional geometric models for detachment folds that form by the end-member processes of hinge migration and limb rotation. These area-balanced models differ from existing models, however, in that they allow 'hinterland inflation' to occur within the incompetent layer above a sub-horizontal detachment, thereby creating a higher local regional level at the trailing edge (i.e., hinterland) of the detachment fold relative to the foreland. This regional difference across the detachment folds may reflect (1) hinterland uplift due to thickening of the incompetent unit, (2) foreland deflation as material from the incompetent unit moves into the fold core as the fold increases in amplitude, and/or (3) inflation of the hinterland as material from the incompetent unit is squeezed out of the fold core as shortening progresses. While we readily acknowledge that there are multiple ways of producing differences in local regional level across natural detachment folds, this manuscript will focus on models where these differences in local regional levels are assumed to be due to thickness changes in the detachment layer above a sub-horizontal detachment. We illustrate the utility of these models by analyzing the two- and three-dimensional geometry of the western termination of the Nuncios Fold Complex in the Monterrey Salient, Mexico.

2. Model descriptions

Detachment fold models that incorporate hinterland inflation are conceptually similar to models described by Poblet and McClay (1996; their models 1 and 2; see also Wilkerson et al., 2004). Specifically, both models depict the geometry of the folded interface between the incompetent unit and the overlying competent unit as two straight fold limbs and a single flat crest that is parallel to both the underlying detachment and to undeformed layers outside the fold itself (Fig. 2). Competent unit bed length is conserved during fold development for both models because penetrative layer-parallel strain is assumed to be negligible in the competent unit and because shortening is homogeneously distributed throughout the deformed layers (i.e., there is a vertical pin line on the trailing edge). Because material is not permitted to move in or out of the plane of the cross section and because bed length of the competent unit is conserved, the cross-sectional area of the model folds is preserved (Fig. 2).

2.1. Model derivation

The following derivation is similar to that provided in Poblet and McClay (1996) with modifications that incorporate hinterland inflation (refer to Fig. 2). For both models, the uplift of the fold crest can be described by

$$u = L_{\mathrm{b}} \sin(D_{\mathrm{b}}) + h, \tag{1}$$

and

$$u = L_{\mathrm{f}} \sin(D_{\mathrm{f}}) \tag{2}$$

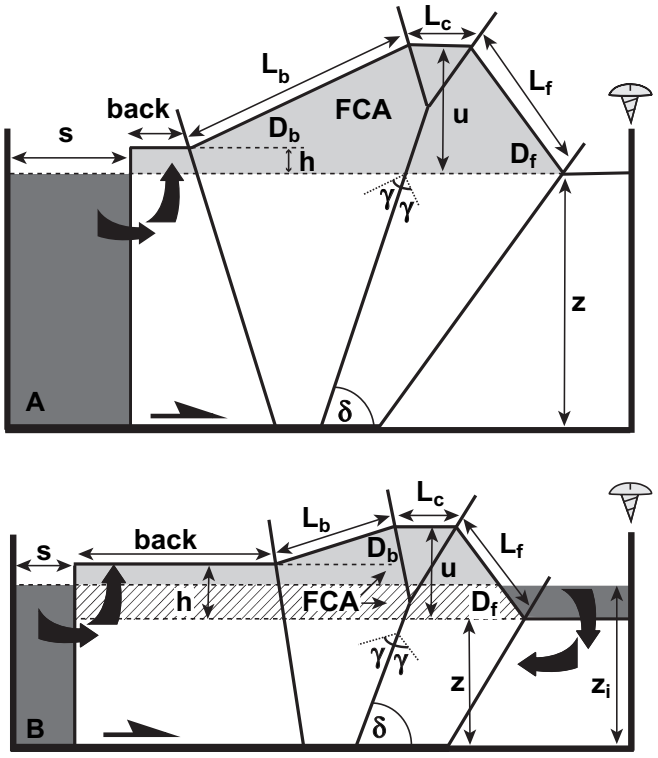

Fig. 2. Idealized hinterland inflation detachment fold models (A, hinge migration; B, limb rotation) with key model parameters labeled. Layer represents the interface between the competent (above) and incompetent units (below). Models are area-balanced. Symbols are as follows: z, detachment depth (z_i, initial detachment depth); s, shortening; D_b, D_f, backlimb and forelimb dips, respectively; L_b, L_f, backlimb and forelimb lengths, respectively; L_c, crest length; u, uplift; h, hinterland uplift; back, distance between the trailing edge and the synclinal axial surface; FCA, uplifted fold core area (A, light gray; B, light gray + diagonal hatch); γ, half-interlimb angle; δ, angle between axial surface and detachment. Dark gray + white is undeformed layer and light gray + white is the deformed layer (dark gray area = light gray area). Arrows emphasize general direction of movement of the incompetent material during folding.

where u is the uplift, h is the hinterland inflation (i.e., difference in elevation between the hinterland and foreland local regional levels outside the bounds of the fold), L_b and L_f are the backlimb and forelimb lengths, respectively, and D_b and D_f are the backlimb and forelimb dips, respectively (see Fig. 2). By setting Eqs. (1) and (2) equal we obtain the relationship for differential fold uplift between the forelimb and backlimb:

$$L_f \sin(D_f) = L_b \sin(D_b) + h, \tag{3}$$

By conserving bed length during the folding process, we can derive a relationship between shortening, bed length, and limb dip (Poblet and McClay, 1996):

$$L_b + L_c + L_f = s + L_b \cos(D_b) + L_c + L_f \cos(D_f) \tag{4}$$

where s is shortening and L_c is the length of the fold crest (see Fig. 2).

Simplifying and rearranging gives:

$$s = L_b[1 - \cos(D_b)] + L_f[1 - \cos(D_f)], \tag{5}$$

Using Fig. 2, we also can derive relationships for the conservation of area between the deformed and undeformed states. Specifically, the uplifted area (FCA) can be described by:

$$\mathrm{FCA} = \frac{(u-h)L_b \cos(D_b)}{2} + \frac{(u)L_f \cos(D_f)}{2} + (u)L_c + h(back + L_b \cos(D_b)) \tag{6}$$

where *back* is the distance between the trailing edge and the synclinal axial surface (see Fig. 2). Substituting Eqs. (1) and (2) into Eq. (6) gives the following expression for the uplifted area:

$$\mathrm{FCA} = \frac{(L_b)^2 \sin(D_b)\cos(D_b)}{2} + \frac{(L_f)^2 \sin(D_f)\cos(D_f)}{2} + L_c L_f \sin(D_f) + h(back + L_b \cos(D_b)) \tag{7}$$

Eqs. (3), (5), and (7) govern the kinematics of models with hinterland inflation and either hinge migration (Fig. 2A) or limb rotation (Fig. 2B).

2.2. Model definition

Definition of both models is similar to that described by Wilkerson et al. (2004) for computer models designed to simulate limb rotation and hinge migration detachment folds. In particular, the length of the cross section, the position of the fault tip, the length of the detachment fold crest, the shortening, and the hinterland inflation are prescribed for both models (Fig. 2). In addition, the lengths of the forelimb and backlimb and the initial detachment depth must be provided for the limb rotation model, and the dips of the forelimb and backlimb must be defined for the hinge migration model (Fig. 2). From these data and the model equations/assumptions previously discussed, area-balanced models may be generated that predict detachment depth for each detachment fold model type.

Many of these variables (e.g., forelimb/backlimb dips and lengths, shortening, fold crest length, etc.) may be readily estimated or measured from natural structures. However, definition of model boundaries and the location of the fault tip is an important and deceptively difficult process (Bulnes and Poblet, 1998; Wallace and Homza, 1998; Wilkerson et al., 2004). Specifically, the cross-section length directly influences the area of the incompetent unit, the amount of material experiencing hinterland inflation, and ultimately the final detachment depth (Fig. 3; also see discussions by Bulnes and Poblet, 1998 (see their Fig. 1); Wallace and Homza, 1998; Wilkerson et al., 2004 for models without hinterland inflation). Fig. 3 shows the change of detachment depth in response to changes in cross-section length for an example detachment fold created by the limb rotation with hinterland inflation model with constant shortening. While the differences in detachment depth are relatively small, there clearly is a corresponding decrease in detachment depth with decreasing cross-section length for the constant shortening

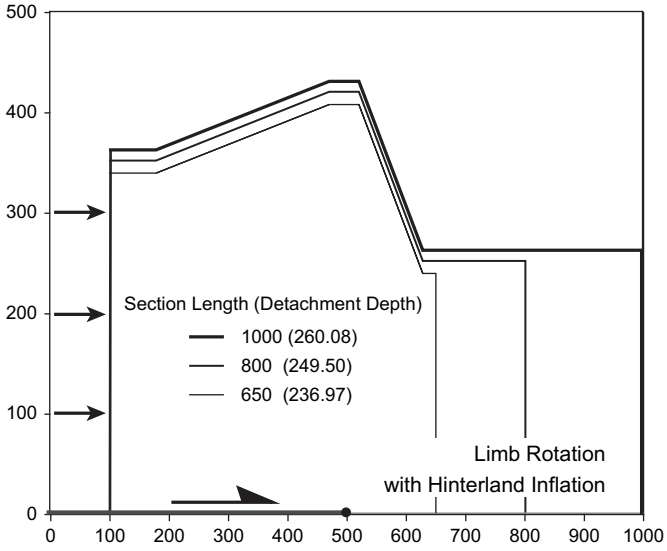

Fig. 3. Effect of cross-section length on detachment depth for a limb rotation model with hinterland inflation. Decreasing cross-section lengths of 1000, 800, and 650 produce corresponding decreases in detachment depths of 260.08, 249.50, and 236.97, respectively (all units are arbitrary). Section vertically exaggerated to emphasize differences in detachment depth. Fault tip placement = 500, fold crest length = 50, forelimb length = 200, backlimb length = 300, shortening = 100, initial detachment depth = 300, and hinterland inflation = 100.

shown (~1% decrease in detachment depth for a 20% decrease in section length; Fig. 3). Bulnes and Poblet (1998) and Wallace and Homza (1998) note similar issues, provide an excellent discussion of the pitfalls associated with placement of boundaries in earlier detachment fold models, and describe the resulting impact on the calculation of detachment depth. Wallace and Homza (1998) suggest that one approach is to assume no flow of material through synclinal hinges and to use these hinges as boundaries for model detachment fold cross sections. While in principle this choice is an objective approach for defining model cross-section boundaries, in practice it may be difficult to definitively locate these boundaries because of exposure and/or fold geometry (Bulnes and Poblet, 1998). Because of this limitation, users must realize that the calculated detachment depth for the models is an approximation that is based on a series of underlying assumptions. As such, it is far more likely that these models will only provide insight into how a particular natural fold developed and a range of possible detachment depths, rather than providing detailed fold kinematics and absolute detachment depth values in areas lacking sufficient data (see also discussion in Wallace and Homza, 1998). Lastly, because both models presented in this paper are pinned on the foreland edge of the cross section, placement of the fold in the cross section relative to the fault tip directly influences material paths during sequential development of the fold (Fig. 4). Care must be taken when modeling natural structures to insure that model material paths are consistent with field observations (Wilkerson et al., 2004).

2.3. Model discussion

Fig. 4 shows the sequential development of limb rotation and hinge migration detachment fold models, both with and without hinterland inflation. It is important to note that for a given set of models in Fig. 4, all variables with the exception of shortening were kept constant. As a consequence, all models have constant fold crest lengths and all hinterland inflation models exhibit a constant local regional difference across the fold (i.e., the sequential development of broadening fold crests and/or of increasing hinterland inflation was not included in the models).

The original limb rotation model (Fig. 4A), which was first described by De Sitter (1956) and described in detail by Poblet and McClay (1996), involves the rigid rotation of fold limbs about fixed fold hinges. In this model, the limb lengths are prescribed at the onset of deformation and with increased shortening, the limbs rotate from gentle to steeper dips (Fig. 4A). In addition to developing steeper dips with increased shortening, the interlimb angle and axial surface dips of the fold also decrease and the detachment depth varies (initially decreasing for shortening values <5%, but subsequently increasing as shortening increases; Homza and Wallace, 1997; Wilkerson et al., 2004). Detachment fold models that develop by limb rotation with hinterland inflation are produced as ductile material moves into the fold core from both the hinterland and foreland with increased shortening (Fig. 2B and 4B; note that this material path is simply a construct of the model and may be different in natural structures). Such detachment fold models develop similarly to models of detachment folds with limb rotation that do not exhibit hinterland inflation (Fig. 4B), with the exception that there is no initial decrease in detachment depth (even for small amounts of shortening). When hinterland inflation occurs in conjunction with limb rotation, detachment depth continuously increases with increased shortening. Lastly, cross sections for both models (Fig. 4A,B) are area-balanced both individually and as shortening changes (i.e., there is constant area from section to section as shortening increases).

The original hinge migration model (Fig. 4C), described conceptually by Mitchell and Woodward (1988) and in detail by Poblet and McClay (1996), assumes that fold kinematics are controlled by hinge migration. These folds evolve with constant limb dips and interlimb angles and accommodate increased shortening by material moving through the axial surfaces and consequently lengthening the fold limbs (Fig. 4C). If the limb dip is maintained and cross-sectional area is held constant, detachment depth increases with increased shortening (Homza and Wallace, 1995; Wilkerson et al., 2004). Detachment fold models that develop by hinge migration with hinterland inflation are produced by movement of ductile material from the hinterland portions of the incompetent unit (Fig. 2A and 4D), producing an elevated hinterland relative to the undeformed foreland regional level. Again, such a material path is a model construct; in natural structures other material migration paths that involve the foreland are certainly possible. In contrast to the limb rotation models, the development of hinge migration detachment fold models that incorporate hinterland inflation is

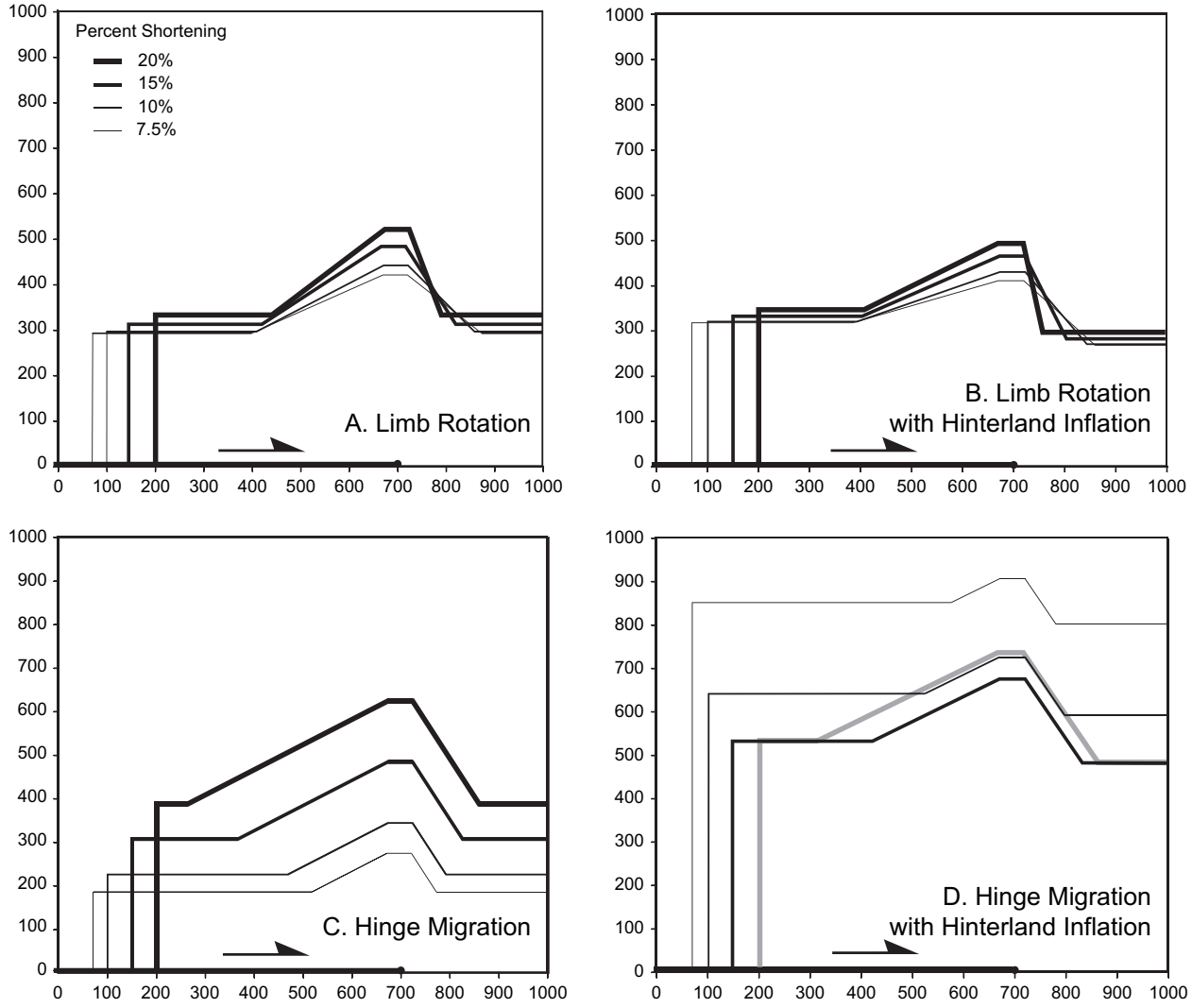

Fig. 4. Sequential development of model detachment folds with increasing shortening (A, limb rotation; B, limb rotation with hinterland inflation; C, hinge migration; D, hinge migration with hinterland inflation; A and C modified from Poblet and McClay, 1996; Wilkerson et al., 2004). Shortening increases from 7.5% (thinnest line) to 20% (thickest line; semi-transparent in D because of overlapping lines). For all models (A–D), cross-section length = 1000, fault tip placement = 700, and fold crest length = 50. For limb rotation models (A and B), forelimb length = 200, backlimb length = 300, and initial detachment depth = 300. For hinge migration models (C and D), forelimb dip = 60° and backlimb dip = 30°. For hinterland inflation models (B and D), hinterland inflation = 50. Units are arbitrary.

quite different than their counterparts without hinterland inflation. Specifically, small amounts of shortening initially produce large detachment depths (Fig. 4D). With increasing shortening, however, detachment depth subsequently decreases and then gradually begins to increase (Fig. 4D). Although individual cross sections are area-balanced, the cross-sectional area changes from section to section as the detachment depth changes (Homza and Wallace, 1995).

3. Application of hinterland inflation models to a natural detachment fold

3.1. Geologic overview

The Nuncios Fold Complex comprises the western termination of the frontal fold in the Laramide-age Monterrey Salient of the Sierra Madre Oriental of northeastern Mexico (Fig. 5, box; Higuera-Diaz et al., 2005). A detailed discussion of the geology, including the stratigraphy, tectonic history, and interpreted structural geometry of the Nuncios Fold Complex, is provided by Higuera-Diaz et al. (2005), and the references therein.

To summarize, the Nuncios Fold Complex reflects the basic geometry of other folds in the Monterrey Salient in that it is a kink-style box fold that is generally symmetric and upright to slightly north-vergent (Fig. 6; see also Higuera-Diaz et al., 2005, their Fig. 9). Although overall the western termination of this frontal first-order fold plunges to the west, it is actually comprised of two second-order, west-plunging anticlines (the Los Muertos and San Blas Anticlines) and an intervening east-plunging syncline (the Sierra Urbano Syncline; Figs. 5 and 6; Higuera-Diaz et al., 2005). Although no outcrop exposures exist of the actual detachment, observations and

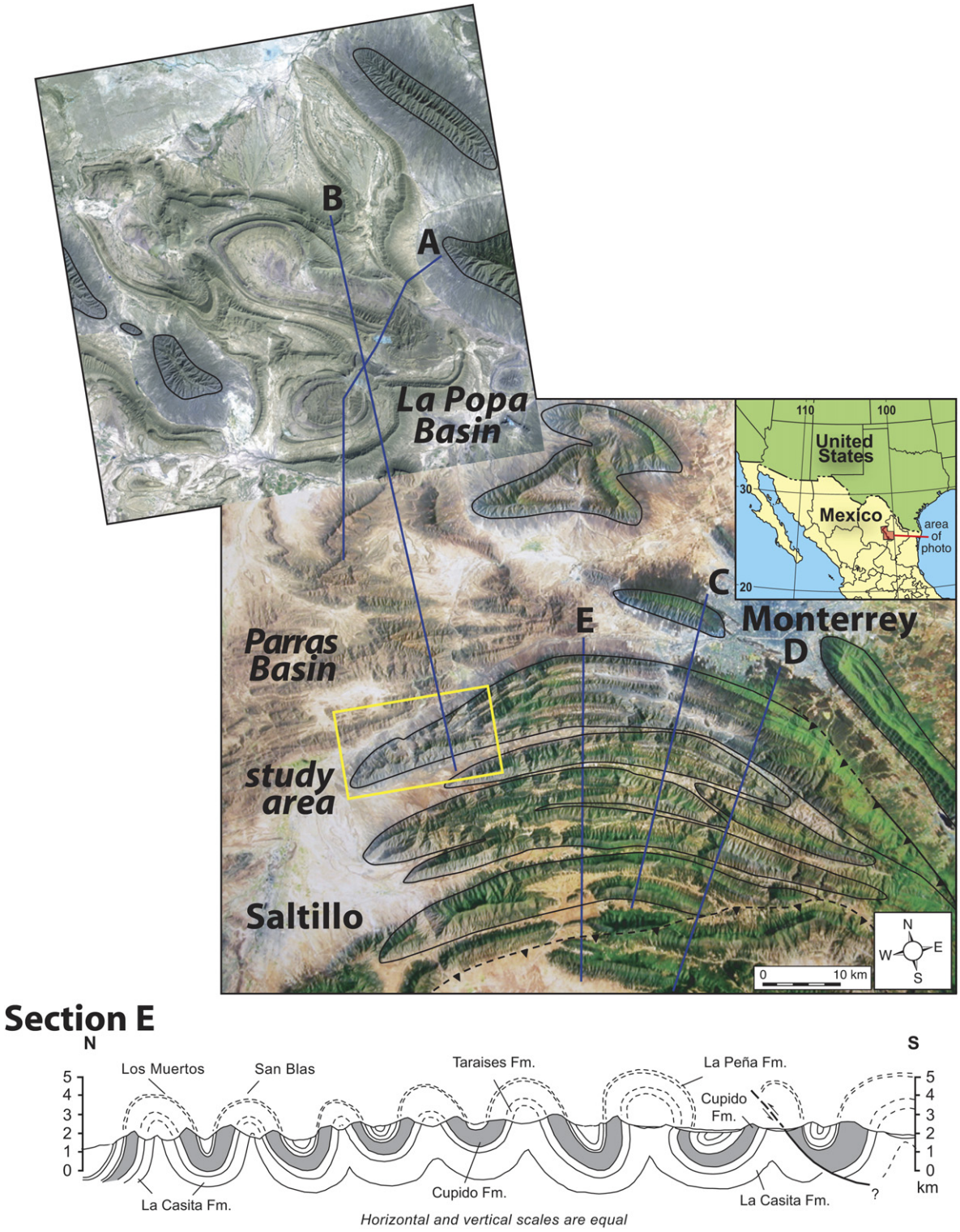

Fig. 5. Satellite photo of the Monterrey Salient, Mexico and surrounding areas (box denotes study area). Lines A–E indicate approximate locations for cross section below photo (line E; after original by Padilla y Sanchez (1982)) and cross sections in Fig. 8. Heavy black lines depict the approximate location of the top of the Aurora Formation and its regional stratigraphic equivalents (see Fig. 7 for stratigraphic column). Heavy black lines with triangles show the approximate locations of thrust faults interpreted by Padilla y Sanchez (1982; triangles on hanging wall). Location map and section modified from Higuera-Diaz et al. (2005).

interpretations of the Nuncios Fold Complex and other folds in the Monterrey Salient suggest that they are evaporite-cored detachment folds involving Upper Jurassic through Cretaceous rocks that deformed during the Laramide Orogeny (Figs. 5 and 6; e.g., Humphrey, 1949; De Cserna, 1956; Padilla y Sanchez, 1982; Fischer and Jackson, 1999; Goldhammer and Wilson, 1999; Marrett and Aranda-Garcia, 1999; Gray et al., 2001; Millán-Garrido, 2004; Higuera-Diaz et al., 2005).

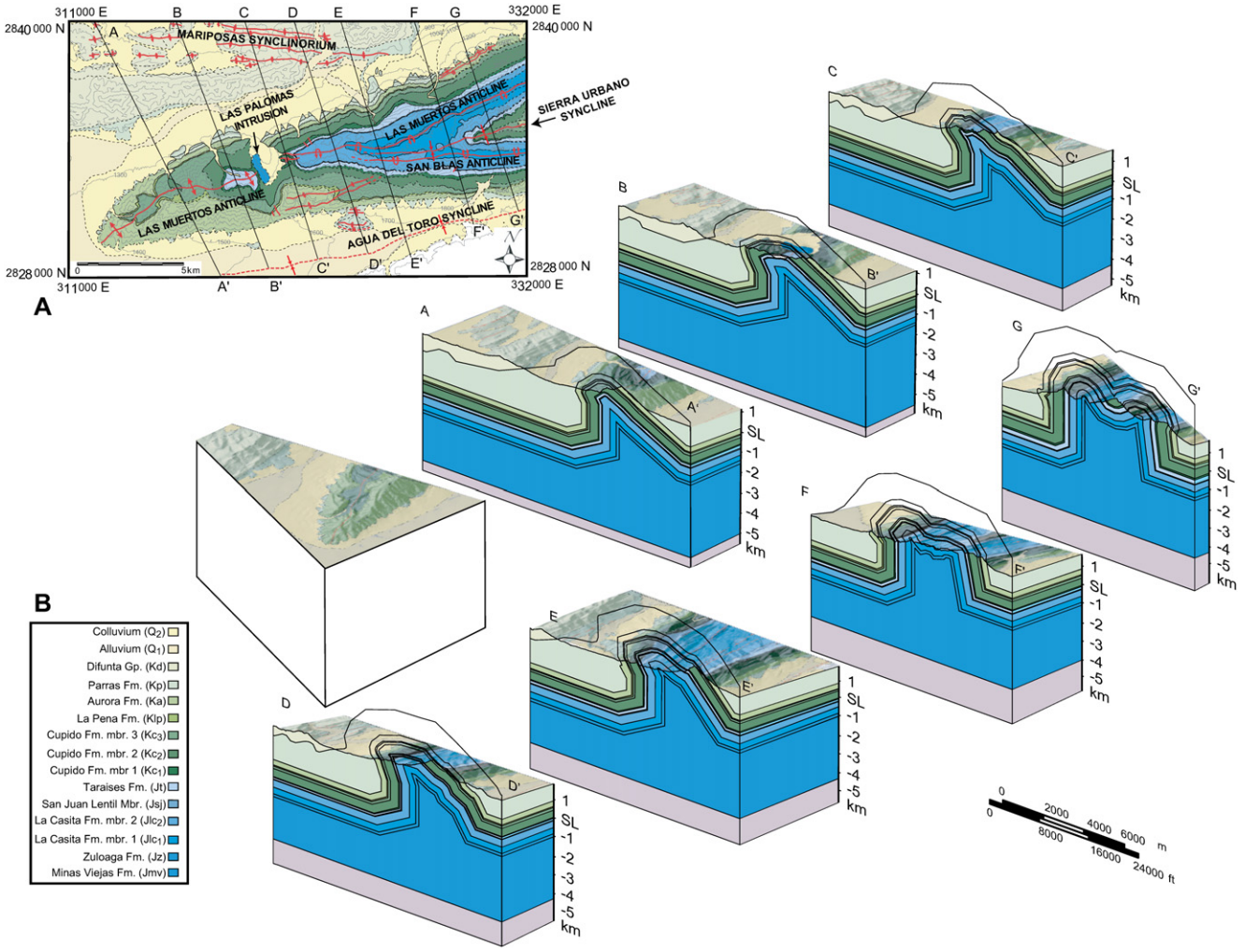

Fig. 6. Geology of the Nuncios Fold Complex (modified from Higuera-Diaz et al., 2005). (A) Geologic map with serial cross-section lines AA′–GG′ shown. (B) Serial cross sections AA′–GG′ depicted in 'exploded' three-dimensional perspective. Top surface of blocks created by draping geologic map over a digital elevation model of the region. Color key provides correlations for units shown in Fig. 7 (see Higuera-Diaz et al., 2005 for detailed stratigraphy).

Fig. 7 shows a stratigraphic column for the region with generalized rock descriptions (adapted from Higuera-Diaz et al., 2005, and references therein). These stratigraphic layers may be grouped into four lithotectonic units (LTU's) based on their competencies and general mechanical behavior (Higuera-Diaz et al., 2005; described from oldest to youngest): (1) a weak LTU comprised solely of the Minas Viejas Formation, which consists predominantly of evaporites of unknown thickness that are exposed in the field area as the Las Palomas intrusion (Fig. 6) and to the foreland in the Parras and La Popa Basins as diapiric structures (Fig. 5); (2) an intermediate competency LTU consisting of the Zuloaga, La Casita, and Taraises Formations, which are composed mainly of mixed clastics and carbonates; (3) a relatively high competency LTU comprised of the Cupido, La Peña, Aurora, and Indidura Formations, which are mostly thick-bedded carbonates; and (4) a weak LTU consisting of the Parras Shale and the Difunta Group, both of which are mostly fine-grained clastics (Fig. 7). The mechanical behavior of this stratigraphic sequence is consistent with other regions that exhibit detachment folds.

Because of the lack of subsurface data, a broad spectrum of possible cross-sectional interpretations exists in the literature to describe the detailed geometry and underlying formative mechanisms of the Nuncios Fold Complex and other folds in the Monterrey Salient (Figs. 5 and 8; e.g., De Cserna, 1956; Padilla y Sanchez, 1982; Marrett and Aranda-Garcia, 1999; Gray et al., 2001; Millán-Garrido, 2004). These interpretations range from detachment folds with and/or without specified detachments, detachment folds above tilted/folded basement and/or faulted basement uplifts, and hybrid detachment and other fault-related folds (Figs. 5 and 8). All of these interpretations have different thicknesses and geometries of the incompetent Minas Viejas Formation, which commonly is drawn with an elevated hinterland outside the fold proper (Fig. 8). At present, data simply are not available to constrain which, if any, of these interpretations might be correct, as published seismic data do not exist and published regional magnetic and gravity data are inconclusive. In addition, evidence constraining movement of material in or out of the section plane does not exist to help assess the validity of area-balancing cross sections through the region. Despite

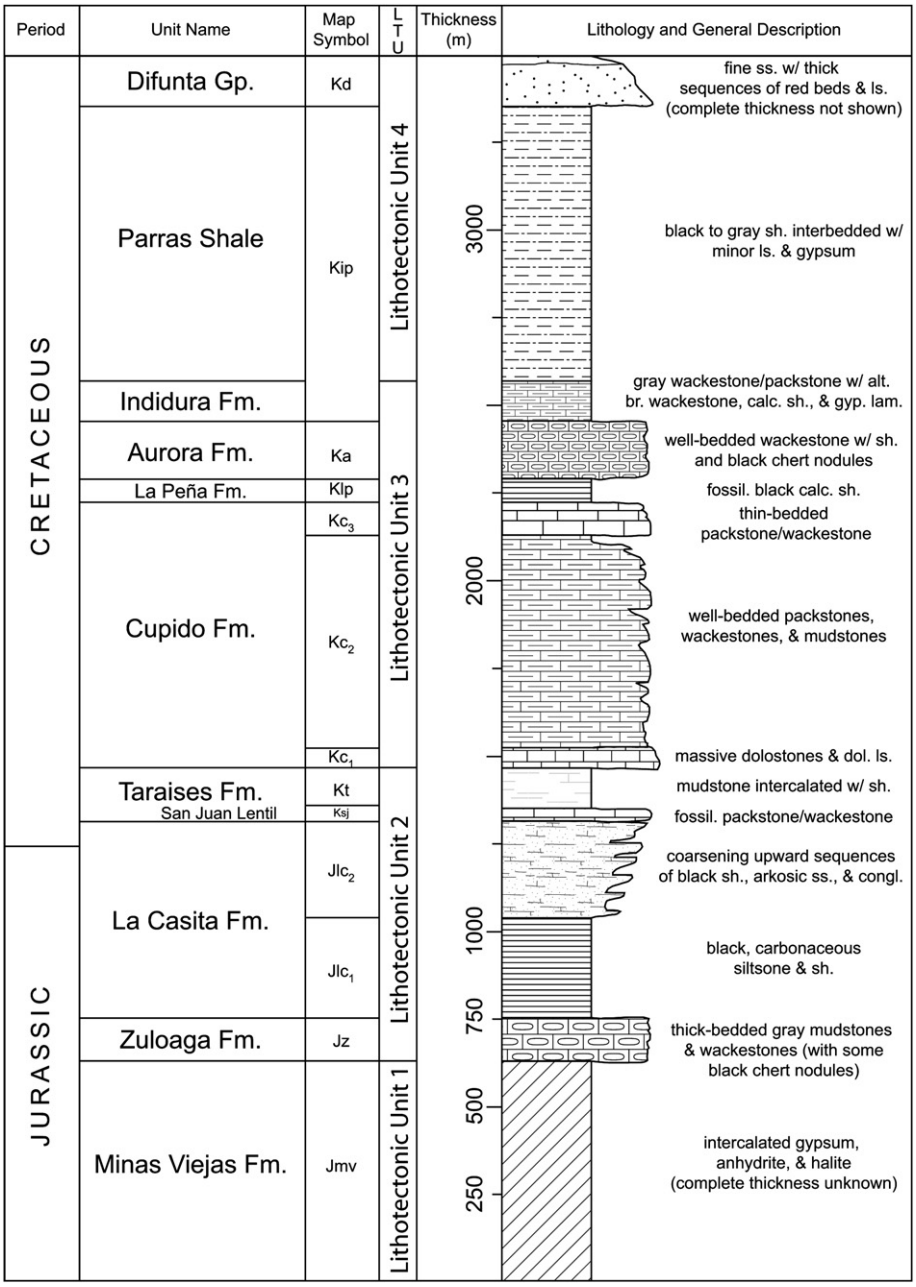

Fig. 7. Stratigraphic column for rocks exposed in the Nuncios Fold Complex field area (and in general throughout the Monterrey Salient). Figure and descriptions adapted from Higuera-Diaz et al. (2005), and references therein.

these data shortcomings, however, the interpretation variability in this region underscores the importance for developing more objective techniques to help constrain subsurface interpretations in this area with respect to the (1) detachment depth, (2) thickness of the incompetent unit, and (3) explanation for the hinterland inflation/uplift observed in several folds.

Higuera-Diaz et al. (2005) attempted to objectively address the first two issues by using the Epard and Groshong (1993) depth-to-detachment technique to constrain the depth of the detachment, and therefore the thickness of the incompetent unit. In so doing, Higuera-Diaz et al. (2005) noted that the Epard and Groshong (1993) depth-to-detachment technique requires that the undeformed local regional level be the same across the fold. To address this requirement and yet incorporate the elevated hinterland regionals of the competent units (i.e., hinterland inflation) observed in the Nuncios Fold Complex, they (1) assumed a horizontal, undeformed regional level using estimates derived from projecting stratigraphic thicknesses to depth beneath the Mariposas Synclinorium on the northern (i.e., foreland) side of the fold (Fig. 6), (2) measured excess areas above this regional level that incorporated not only the uplifted fold core area, but also the area experiencing hinterland inflation (essentially FCA in Fig. 2A), (3) assumed a horizontal detachment parallel to the horizontal regional level for each

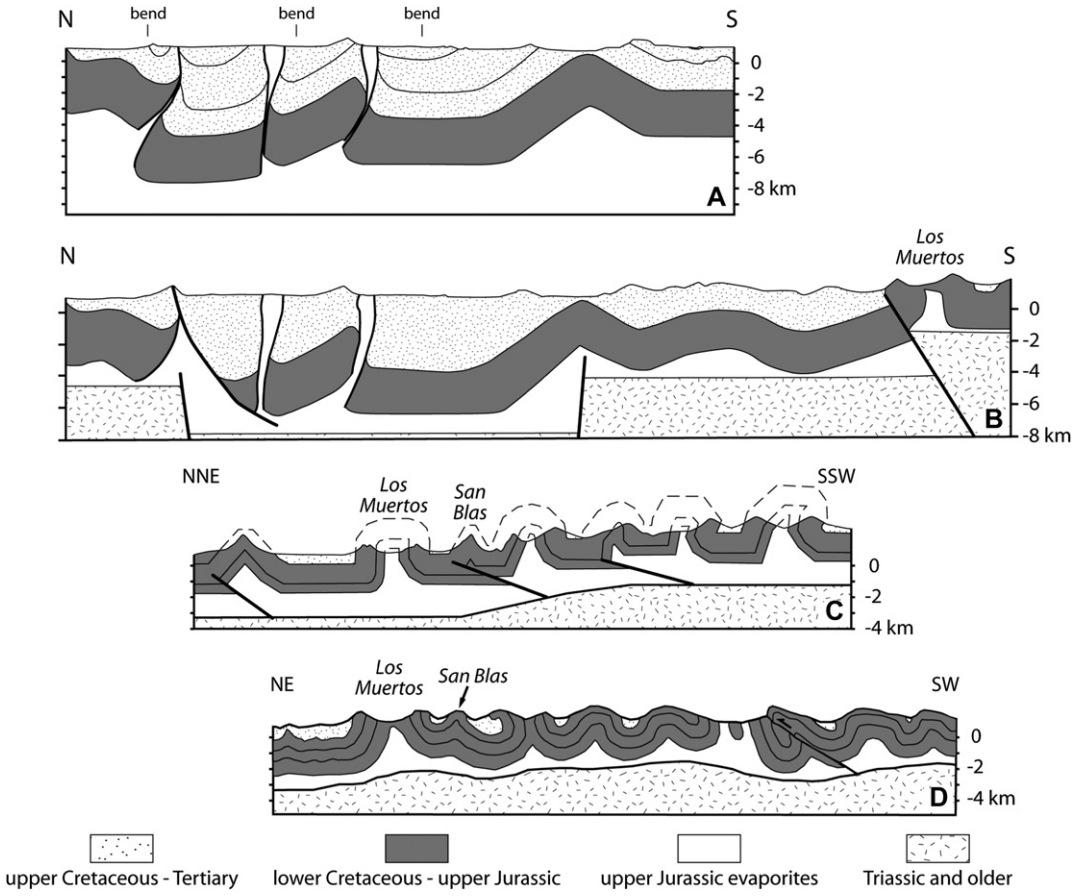

Fig. 8. Published regional cross sections through the Monterrey Salient (after Higuera-Diaz et al., 2005). Sections from: A, Millán-Garrido (2004); B, Gray et al. (2001); C, Marrett and Aranda-Garcia (1999); D, De Cserna (1956). Approximate section locations shown in Fig. 5.

unit, and (4) assumed a horizontal sub-detachment basement (Higuera-Diaz et al., 2005). Higuera-Diaz et al. (2005) suggested that their ad hoc application of Epard and Groshong's (1993) technique would likely lead to calculated detachment depths that represent a maximum because they used the foreland part of the structure to establish the regional level for the excess area measurements rather than the shallower hinterland part of the structure (a shallower regional level would have produced a smaller excess area and a correspondingly shallower detachment depth). Results from Higuera-Diaz et al.'s (2005) calculations suggest that the detachment depth for the western termination of the Nuncios Fold Complex may vary from approximately −3.5 km in the east to as deep as −5.2 km in the west, describing a three-dimensional detachment geometry that dips ∼07° towards an azimuth of ∼252°.

3.2. Modeling methodology

To explore the utility of Higuera-Diaz et al.'s (2005) application of Epard and Groshong's (1993) technique to constrain the detachment depth of the Nuncios Fold Complex, and to investigate the possibility that the western termination of the Nuncios Fold Complex developed hinterland inflation by changes in the incompetent layer above a sub-horizontal detachment, the two new models with hinterland inflation were used to model the Nuncios Fold Complex.

To begin the modeling process, the interpreted fold geometry of the top of the incompetent unit (the Minas Viejas Formation) in each cross section in Fig. 6 was modeled using DETACH™, a Microsoft Excel™ program that we created to model detachment folds (Wilkerson et al., 2004). Models were created for each of Higuera-Diaz et al.'s (2005) cross sections (Fig. 6A–G) by specifying cross-section length, fault tip placement within the cross section (here, the center of the fold crest), fold crest length, shortening, hinterland inflation (local to the Nuncios Fold Complex), forelimb/backlimb lengths (limb rotation models only), initial detachment depth (limb rotation models only), and forelimb/backlimb dips (hinge migration models only). Values for these inputs were measured directly from each of Higuera-Diaz et al.'s (2005) cross sections (Fig. 6A–G) by approximating the fold itself with two planar fold limbs and a horizontal fold crest (bold line in Fig. 9). Initial detachment depths, necessary for the limb rotation models only, were iteratively adjusted to create a best-fit geometry between the models and Higuera-Diaz et al.'s (2005) interpreted fold geometry. After input of these data, DETACH™ produced area-balanced cross sections of the model geometry of the top of the incompetent unit for the specified

fold kinematics as well as the model detachment geometry positioned at the calculated detachment depth.

As discussed previously, constraining these input parameters to model natural detachment folds is subject to several possible difficulties. Specifically, Higuera-Diaz et al.'s (2005) interpreted cross sections (Fig. 6) were produced from detailed field mapping of the exposed Nuncios Fold Complex (Fig. 6A) and then stratigraphic units were projected downward and into the adjacent synclines beneath areas that are largely covered. As such, the amount of local hinterland inflation is subject to the accuracy of this projection/interpretation. Similarly, the lengths of Higuera-Diaz et al.'s (2005) cross sections are not constrained by significant material boundaries (e.g., syncline axial surfaces, Wallace and Homza, 1998), which would be difficult to delimit in any case, given the sedimentary cover and the observation that the Nuncios Fold Complex is one of a train of folds that exhibits hinterland inflation (see Fig. 8). As shown earlier, changes in cross-section length can produce changes in detachment depths on the order of an ~1% decrease in detachment depth for a 20% decrease in section length (Fig. 3), so any calculated detachment depth is only a first-order approximation. In addition, because the Nuncios Fold Complex is one of a series of folds that appear to possess overlapping zones of deformation with neighboring folds, a better constrained cross section might be obtained after detailed study of a regional transect in order to more accurately establish an undeformed regional, better constrained pin lines, etc. Lastly, the original cross sections (and the hinterland inflation models) assume no movement of material in or out of the section plane. This assumption may or may not be valid given the evaporitic nature of the Minas Viejas Formation and the fact that these sections pass through the plunging western termination of the Nuncios Fold Complex. Although undoubtedly incorrect in detail and with the realization that this approach cannot mirror every geometrical feature of the Nuncios Fold Complex, we believe that using these models provides an objective means of obtaining a first-order best fit of the overall fold geometry and determining if end-member limb rotation and hinge migration models with hinterland inflation yield realistic detachment depths and reasonable interpretations for the Nuncios Fold Complex.

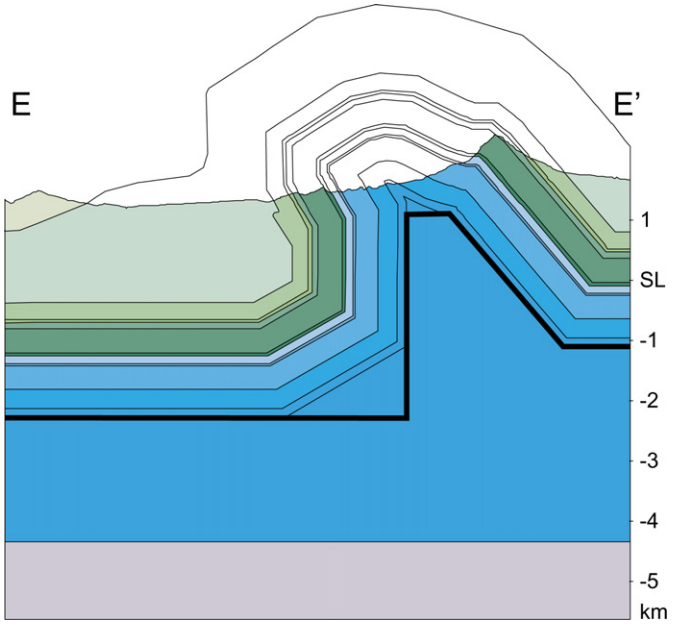

Fig. 9. Approximation of each Nuncios Fold Complex cross section with model geometry.

Once limb rotation and hinge migration models with hinterland inflation were created for each of these serial cross sections (along lines A–G in Fig. 6), they were subsequently imported into the Geosec2D™ cross-section modeling program to project the stratigraphic thicknesses to other horizons and to locate the serial sections in their proper three-dimensional spatial reference frame. For the former, we projected stratigraphic thicknesses assuming parallel folding within the section, but allowed variable thicknesses from section to section (approach used by Higuera-Diaz et al.'s (2005) interpreted cross sections as constrained by field exposures; Fig. 6B). The thickness of the incompetent unit is unknown and was only shown down to the detachment (Fig. 6B). For the latter, section lines were oriented and properly positioned to correspond with Higuera-Diaz et al.'s (2005) interpreted section lines A–G as shown in Fig. 6A.

We then exported the final serial sections to the Gocad™ three-dimensional modeling software. Within Gocad™, pseudo-three-dimensional surfaces for each horizon and the detachment were constructed from the serial sections (cf. Wilkerson et al., 1991). Links from section to section placed constraints on Gocad™'s surface tessellation algorithm such that the final surfaces could be smoothed and yet still honor along-strike dip domains for the fold. Once all surfaces were constructed, the resultant 3-D models were contoured to provide detailed structure-contour maps for comparison with the actual interpretation (Fig. 10A) and were sliced to provide additional cross sections at any orientation and/or to 'erode' the model for comparison with the actual geologic map of the area (Fig. 10B).

3.3. Comparison of models to natural structure

Fig. 10A compares both hinterland inflation models with Higuera-Diaz et al.'s (2005) interpreted geometry of the Nuncios Fold Complex. Fig. 10A shows two horizons: the top row represents the top of the competent unit (the Aurora Formation), whereas the bottom row shows the top of the incompetent unit (the Minas Viejas Formation). The latter was modeled using measurements derived from the original cross sections and input into DETACH™, whereas the former was a constant-thickness projection in Geosec2D™ using stratigraphic thicknesses supplied by Higuera-Diaz et al. (2005). The first column in Fig. 10A illustrates the actual three-dimensional interpretation of the surfaces (no detachment is shown) derived from field work and balanced cross sections by Higuera-Diaz et al. (2005). The second and third columns show the three-dimensional models generated for the limb rotation and hinge migration models with hinterland inflation, respectively (Fig. 10A; detachment is shown). All

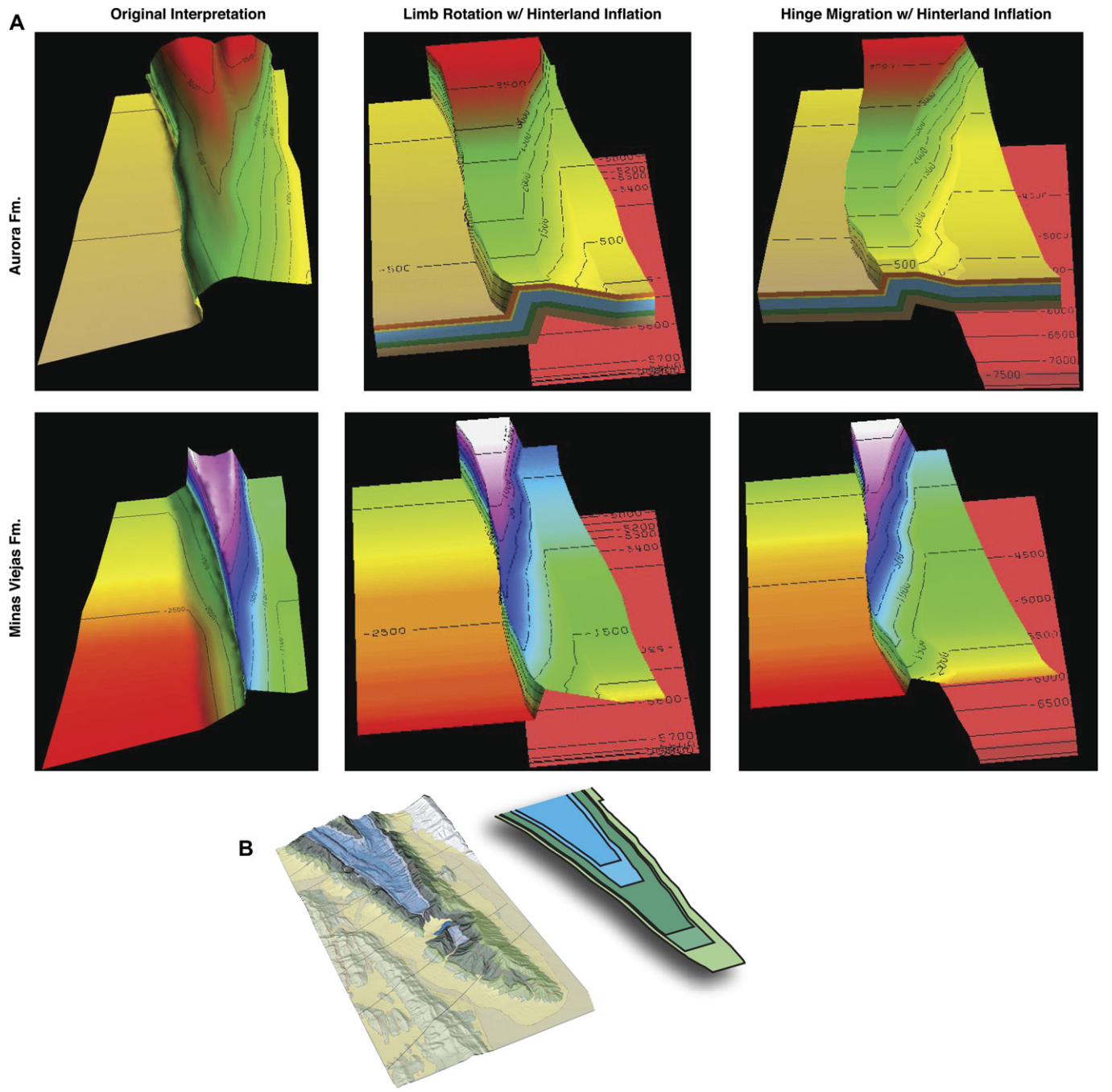

Fig. 10. Model comparison. (A) Comparison of 3-D surfaces of the Nuncios Fold Complex (first column) with model-generated 3-D surfaces for limb rotation with hinterland inflation (second column) and for hinge migration with hinterland inflation (third column). Length of model parallel to transport direction is 16,111 m (limb rotation model) and 17,000 m (hinge migration model). Detachment contours range from −5000 m to −5900 m (limb rotation model) and from −4100 m to −8000 m (hinge migration model). Color scale for row 1 is −880 m to 3820 m, and for row 2 is −3000 m to 1600 m. (B) Comparison of actual geologic map of the Nuncios Fold Complex (left) with horizontal map slice through limb rotation with hinterland inflation model (right).

three-dimensional models have structure contours of that specific horizon draped on the modeled surfaces.

Given that the input data are based on a model approximation (Fig. 9), that the fold limb lengths (hinge migration model) and fold limb dips (limb rotation model) are dependent on other variables in the models (especially shortening), and that the models illustrate fold development using different kinematic processes, the models match Higuera-Diaz et al.'s (2005) interpreted fold geometries very well (Fig. 10A). Specifically, the following first-order features observed in the original interpretation are reflected in the models: (1) the axial surfaces show a slight curvature towards the fold termination, (2) limb dips are relatively gentle near the fold termination, but become steep to overturned towards the center of the fold, and (3) the areas outside the fold proper exhibit similar amounts of hinterland inflation and dip to the west

(Fig. 10A). Not only is the geometric match reasonably good, but the models also predict realistic along-strike changes in displacement for the trailing edge of the structure (Fig. 10A; cf. Wilkerson, 1992). The models do not entirely reproduce the interpreted changes in the fold from an asymmetric kink fold at the termination to a complex box fold with a crestal syncline toward the center because of the dip-domain limitations imposed by the model geometries. Nonetheless, most first-order geometrical features are present and reproduced accurately. To support this assertion, we also created horizontal slices through the models to allow comparison of the actual geologic map (Higuera-Diaz et al., 2005) with model geologic maps (Fig. 10B; only limb rotation model with hinterland inflation shown). Again, there was excellent overall agreement on major first-order features between the actual geologic map and its 'eroded' model equivalents.

Both models predict a detachment that dips towards the west in the direction of fold plunge (Fig. 10A). Specifically, the limb rotation model with hinterland inflation predicts a shallow dip of $\sim 03^\circ$ towards the west, whereas the hinge migration model with hinterland inflation predicts a much larger dip of $\sim 13^\circ$. This difference in dip between the models is reflected in a significant difference in calculated along-strike detachment depths. Namely, the limb rotation model produces along-strike detachment depths roughly similar to area-balanced calculations performed by Higuera-Diaz et al. (2005) using the Epard and Groshong (1993) technique. The hinge migration model, however, predicts much deeper detachment depths along strike, culminating in an unrealistically deep detachment depth of -8000 m near the western termination. Such a detachment depth is significantly greater than estimated maximum thicknesses published for the Minas Viejas Formation in the Monterrey Salient or in the surrounding Parras and La Popa Basins (McBride et al., 1974; Rowan et al., 2003; Millán-Garrido, 2004).

4. Discussion

Field observations by Fischer and Jackson (1999), Higuera-Diaz (2005) and by Higuera-Diaz et al. (2005) support the observation that the limb rotation model with hinterland inflation provides a more reasonable estimate for detachment depth of the western termination of the Nuncios Fold Complex than the hinge migration model with hinterland inflation. Specifically, they observe that mesoscopic structures exposed in the Nuncios Fold Complex are consistent with fixed-hinge, fixed-limb-length, rotating-limb kinematics. Based on our modeling and these field observations, the limb rotation model with hinterland inflation appears to be the better fit of the two end-members to describe the overall fold kinematics and to help constrain the detachment depth of the Nuncios Fold Complex.

We should note, however, that many other detachment fold models exist (e.g., hybrid limb rotation and hinge migration models, models with variable limb thicknesses, etc.; cf. Wilkerson et al., 2004) that may produce equally viable geometric fits to the Nuncios Fold Complex, yet quite different detachment depths. Moreover, any such pseudo-three-dimensional approach would be suspect if significant out-of-plane motion of material has occurred. However, we suggest that the usefulness of this approach lies in that it provides an objective means of using surface geology and area-balanced kinematic models to constrain first-order subsurface interpretations. As such, we would suggest that the depths predicted by our modeling reasonably approximate realistic detachment depths for the Nuncios Fold Complex, providing it developed by the hinterland inflation model proposed here.

5. Conclusions

Existing geometric and kinematic models of detachment folds most commonly use the kinematic processes of hinge migration, limb rotation, or some combination of the two to create 2-D, area-balanced cross sections of detachment folds (e.g., Dahlstrom, 1990; Homza and Wallace, 1995, 1997; Poblet and McClay, 1996; Atkinson and Wallace, 2003). Such models are created by prescribing geometric relationships between shortening, detachment depth, limb dips, and limb lengths while maintaining a constant regional stratigraphic level outside the fold itself. While such models have great utility, they cannot adequately describe folds like the Nuncios Fold Complex near Monterrey, Mexico where the hinterland regional is higher than the foreland regional, producing hinterland inflation. This regional difference across the detachment fold potentially could develop for many reasons, such as thickening of the incompetent unit in response to shortening, foreland deflation as material from the incompetent unit moves into the fold core during fold growth, and/or inflation of the hinterland as material from the incompetent unit is squeezed out of the fold core with increased shortening.

We derived two new models that incorporate hinterland inflation, one using hinge-migration kinematics and the other using limb-rotation kinematics. To test the utility of these models, we compared two- and three-dimensional synthetic models with interpretations from the Nuncios Fold Complex. The geometric agreement between both two- and three-dimensional models and the interpretation was qualitatively very good. However, the limb rotation model that incorporated hinterland inflation best fits the interpreted data and provides better constraints on detachment depth than does its hinge migration counterpart, which requires an unrealistically deep detachment. These results (1) lend further support to the interpretation that limb rotation was the dominant kinematic mechanism in the development of the Nuncios Fold Complex, (2) may help constrain the approximate depth and dip of the detachment underlying the Nuncios Fold Complex, and (3) provide a reasonable two-dimensional and pseudo-three-dimensional balanced interpretation of the Nuncios Fold Complex that may provide insight into its structural development.

Acknowledgements

The authors are indebted to Paradigm Geophysical, Inc. for the use and support of the Geosec2D™ structural modeling software, and to Earth Decision Sciences for the use of the Gocad™ 3-D modeling software. Support for this work was provided by

NSF grant EAR-9972993 to M. Fischer and E. Perry (and by an NSF-ROA supplement to this grant to Wilkerson). The Science Research Fellows and the Faculty Development Programs at DePauw University also supported Wilkerson, Smaltz, and Bowman. The authors benefited greatly from source code donated by Dr Josep Poblet and from the programming skills of Josh Wilson. Reviews by Wes Wallace and Ryan Shackleton greatly improved the quality of the manuscript.

References

Apotria, T.G., Wilkerson, M.S., 2002. Seismic expression and kinematics of a fault-related fold termination: Rosario Structure, Maracaibo Basin, Venezuela. Journal of Structural Geology 24 (4), 671–689.

Atkinson, P.K., Wallace, W.K., 2003. Competent unit thickness variation in detachment folds in the northeastern Brooks Range, Alaska: geometric analysis and a conceptual model. Journal of Structural Geology 25 (10), 1751–1771.

Bulnes, M., Poblet, J., 1998. Detachment folds with fixed hinge and variable detachment depth, northeastern Brooks Range, Alaska. Discussion. Journal of Structural Geology 20 (11), 1587–1590.

Chamberlin, R.T., 1910. The Appalachian folds of central Pennsylvania. Journal of Geology 18, 228–251.

Dahlstrom, C.D.A., 1970. Structural geology in the eastern margin of the Canadian Rocky Mountains. Bulletin of Canadian Petroleum Geology 18 (3), 332–406.

Dahlstrom, C.D.A., 1990. Geometric constraints derived from the law of conservation of volume and applied to evolutionary models for detachment folding. American Association of Petroleum Geologists Bulletin 74 (3), 336–344.

De Cserna, Z., 1956. Tectónica de la Sierra Madre Oriental de México, entre Torreón y Monterrey. Paper presented at XX Congreso Geológico Internacional, Inst. Nac. para la Invest. de Recursos Miner. de México, México City, México.

De Sitter, L.U., 1956. Structural Geology, first ed. McGraw-Hill, New York, 552 pp.

Epard, J.-L., Groshong, R.H., 1993. Excess area and depth to detachment. American Association of Petroleum Geologists Bulletin 77 (8), 1291–1302.

Epard, J.-L., Groshong, R.H., 1995. Kinematic model of detachment folding including limb rotation, fixed hinges, and layer-parallel strain. Tectonophysics 247 (1–4), 85–103.

Fischer, M.P., Jackson, P.B., 1999. Stratigraphic controls on deformation patterns in fault-related folds: A detachment fold example from the Sierra Madre Oriental, northeast Mexico. Journal of Structural Geology 19, 413–441.

Goldhammer, R.K., Wilson, J.L., 1999. Tectonic framework, part 2. In: Wilson, J.L., Ward, W.C., Marrett, R.A. (Eds.), Stratigraphy and Structure of the Jurassic and Cretaceous Platform and Basin Systems of the Sierra Madre Oriental; Monterrey and Saltillo Areas: Northeastern Mexico, A Field Book and Related Papers. Gulf Coast Section, Society of Sedimentary Geologists, Tulsa, OK, pp. 108–110.

Gray, G.C., Pottorf, R.J., Yurewicz, D.A., Mahon, K.I., Pevear, D.A., Chuchla, R.J., 2001. Thermal and chronological record of syn- to post-Laramide burial and exhumation, Sierra Madre Oriental, Mexico. In: Bartolini, C., Buffler, R.T., Cantú-Chapa, J.C. (Eds.), The Western Gulf of Mexico Basin: Tectonics, Sedimentary Basins and Petroleum Systems, 75. American Association of Petroleum Geologists Memoir, pp. 159–181.

Groshong, R.H., Epard, J.-L., 1994. The role of strain in area-constant detachment folding. Journal of Structural Geology 16 (5), 613–618.

Hardy, S., Poblet, J., 1994. Geometric and numerical model of progressive limb rotation in detachment folds. Geology 22 (4), 371–374.

Higuera-Diaz, I.C., 2005, Geometry, kinematics, and paleofluid systems of a detachment fold complex in northeastern Mexico. MS thesis, Northern Illinois University.

Higuera-Diaz, I.C., Fischer, M.P., Wilkerson, M.S., 2005. Geometry and kinematics of the Nuncios detachment fold complex: implications for lithotectonics in northeastern Mexico. Tectonics 24 (4), TC4010. doi:10.1029/2003TC001615.

Homza, T.X., Wallace, W.K., 1995. Geometric and kinematic models for detachment folds with fixed and variable detachment depths. Journal of Structural Geology 17 (4), 575–588.

Homza, T.X., Wallace, W.K., 1997. Detachment folds with fixed hinges and variable detachment depth, northeastern Brooks Range, Alaska. Journal of Structural Geology 19 (3-4), 337–354.

Humphrey, W.E., 1949. Geology of the Sierra de Los Muertos Area, Mexico [with description of Aptian cephalopods from La Peña Formation]. Geological Society of America Bulletin 60, 89–176.

Jamison, W.R., 1987. Geometric analysis of fold development in overthrust terranes. Journal of Structural Geology 9 (2), 207–219.

Marrett, R., Aranda-Garcia, M., 1999. Structure and kinematic evolution of the Sierra Madre Oriental fold-thrust belt. In: Marrett, R.A., Wilson, J.L., Ward, W.C. (Eds.), Stratigraphy and Structure of the Jurassic and Cretaceous Platform and Basin Systems of the Sierra Madre Oriental. South Texas Geological Society, San Antonio, Texas, pp. 69–98.

McBride, E.G., Weidie, A.E., Wolleben, J.A., Laudon, R.C., 1974. Stratigraphy and structure of the Parras and La Popa Basins, northeastern Mexico. Geological Society of American Bulletin 84, 1603–1612.

Millán-Garrido, H., 2004. Geometry and kinematics of compressional growth structures and diapirs in the La Popa Basin of northeast Mexico: insights from sequential restoration of a regional cross section and three-dimensional analysis. Tectonics 23, TC5011. doi:10.1029/2003TC001540.

Mitchell, M.M., Woodward, N.B., 1988. Kink detachment fold in the southwest Montana fold and thrust belt. Geology 16 (2), 162–165.

Mitra, S., 1990. Fault-propagation folds: geometry, kinematics, and hydrocarbon traps. American Association of Petroleum Geologists Bulletin 74 (6), 921–945.

Mitra, S., 1992. Balanced structural interpretations in fold and thrust belts. In: Mitra, S., Fischer, G.W. (Eds.), Structural Geology of Fold and Thrust Belts. John Hopkins University Press, Baltimore, pp. 53–77.

Mitra, S., 2003. A unified model for the evolution of detachment folds. Journal of Structural Geology 25 (10), 1659–1673.

Padilla y Sanchez, R., 1982. Geologic evolution of Sierra Madre Oriental between Linares Concepcion del Oro, Saltillo, and Monterrey, Mexico. PhD thesis, University of Texas, 217 pp.

Poblet, J., Hardy, S., 1995. Reverse modeling of detachment folds: application to the Pico de Aguila anticline in the South Central Pyrenees (Spain). Journal of Structural Geology 17 (12), 1707–1724.

Poblet, J., McClay, K.R., 1996. Geometry and kinematics of single-layer detachment folds. American Association of Petroleum Geologists Bulletin 80 (7), 1085–1109.

Rowan, M.G., Lawton, T.F., Giles, K.A., Ratliff, R.A., 2003. Near-salt deformation in La Popa Basin, Mexico, and the northern Gulf of Mexico: a general model for passive diapirism. American Association of Petroleum Geologists Bulletin 87, 733–756.

Suppe, J., 1983. Geometry and kinematics of fault-bend folding. American Journal of Science 283 (9), 684–721.

Suppe, J., Medwedeff, 1990. Geometry and kinematics of fault-propagation folding. Eclogae Geologicae Helvetica 83 (3), 409–454.

Thomas, W.A., 2001. Mushwad: ductile duplex in the Appalachian thrust belt in Alabama. American Association of Petroleum Geologists Bulletin 85 (10), 1847–1869.

Wallace, W.K., Homza, T.X., 1998. Detachment folds with fixed hinges and variable detachment depth, northeastern Brooks Range, Alaska. Reply. Journal of Structural Geology 20 (11), 1591–1595.

Wilkerson, M.S., 1992. Differential transport and continuity of thrust sheets. Journal of Structural Geology 14 (6), 749–751.

Wilkerson, M.S., Medwedeff, D.A., Marshak, S., 1991. Geometrical modeling of fault-related folds: a pseudo-three-dimensional approach. Journal of Structural Geology 13 (7), 801–812.

Wilkerson, M.S., Wellman, P.C., 1993. Three-dimensional geometry and kinematics of the Gale-Buckeye thrust system, Ouachita fold-thrust belt, Latimer and Pittsburg Counties, Oklahoma. American Association of Petroleum Geologists Bulletin 77 (6), 1082–1100.

Wilkerson, M.S., Wilson, J.M., Poblet, J., Fischer, M.P., 2004. DETACH: an Excel™ spreadsheet to simulate 2-D cross sections of detachment folds. Computers & Geosciences 30, 1069–1077.